scientific reports

OPEN

Phototoxic effects of nonlinear optical microscopy on cell cycle, oxidative states, and gene expression

Xinyi Zhang[1,5], Gabriel Dorlhiac[2], Markita P. Landry[2,3,4] & Aaron Streets[1,2,4✉]

Nonlinear optical imaging modalities, such as stimulated Raman scattering (SRS) microscopy, use pulsed-laser excitation with high peak intensity that can perturb the native state of cells. In this study, we used bulk RNA sequencing, quantitative measurement of cell proliferation, and fluorescent measurement of the generation of reactive oxygen species to assess phototoxic effects of near-IR pulsed laser radiation, at different time scales, for laser excitation settings relevant to SRS imaging. We define a range of laser excitation settings for which there was no significant change in mouse Neuro2A cells after laser exposure. This study provides guidance for imaging parameters that minimize photo-induced perturbations in SRS microscopy to ensure accurate interpretation of experiments with time-lapse imaging or with paired measurements of imaging and sequencing on the same cells.

Advances in optical engineering over the past three to four decades have led to the development of numerous microscopy techniques that pushed the boundary of what can be probed optically in a biological system. Perhaps most prominent among these new techniques has been two-photon excited fluorescence (TPEF) microscopy. TPEF microscopy has been adopted widely as it has allowed for imaging deeper into tissue due to the wavelengths used for excitation[1]. Beyond TPEF microscopy, there is a growing field of other nonlinear optical microscopy techniques. Nonlinear optics deals with a regime where the peak optical power becomes large enough that nonlinear effects become important. Such peak power is provided by modern pulsed lasers operating in the picosecond to femtosecond regime which concentrate power into a very short pulse duration. The nonlinear optical microscopy field has garnered a lot interest in the past decade, as the additional modalities it offers are in many cases label-free. In principle this means that samples can be probed without the introduction of additional dyes, and in many cases without fixation. One such label-free nonlinear optical imaging modality is Stimulated Raman scattering (SRS), which also provides chemical specificity as TPEF in the form of vibrational signatures[2–4]. SRS makes use of two pulsed lasers of chosen frequency such that the difference in their frequencies is equal to the frequency of a molecular vibration of interest. Such vibrations could, for example, be CH_3 stretches, which are most abundant in intracellular proteins. SRS has been used to investigate numerous systems including lipid droplet formation in single cells[5], metabolic activities[6], and brain tumor detection in vivo[7]. When using nonlinear optical microscopy with high-intensity pulsed lasers, such as SRS, it is important to consider the effects of laser exposure on the cells. This is particularly relevant when the microscopy experiment is not the end-point measurement, for example, when imaging is paired with sequencing.

Phototoxicity has been broadly characterized in the context of optical microscopy[8]. In the continuous-wave regime, visible laser radiation has been associated with increase in reactive oxygen species (ROS) and loss of cell viability[9,10]. Imaging with pulsed lasers has also been associated with a decrease of cloning efficiency[11] and membrane blebbing[12], in addition to an increase in ROS and loss of cell viability[13–15]. Yet despite these observations, there lacks a comprehensive study of how laser irradiation alters cell state, on the metabolic and transcriptomic level. Recent advances have provided high-throughput methods to combine RNA-sequencing (RNA-seq) and microscopy on the same cells, such as μCB-seq[16] and SCOPE-Seq[17]. When combining such methods with

[1]Department of Bioengineering, University of California, Berkeley, Berkeley, CA, USA. [2]Biophysics Graduate Group, University of California, Berkeley, Berkeley, CA, USA. [3]Department of Chemical and Biomolecular Engineering, University of California, Berkeley, Berkeley, CA, USA. [4]Chan-Zuckerberg Biohub, San Francisco, CA, USA. [5]Present address: Department of Electrical Engineering and Computer Science, Massachusetts Institute of Technology, Cambridge, MA, USA. ✉email: astreets@berkeley.edu

Exposure conditions	Magnification (NA)	Avg intensity (mW/ μm²)	fluency (J/cm²)	Pixel dwelling time (μs/pixel)	Peak intensity (W/ μm²)
I0-E0	20X (0.75)	48	10	2	4970.45
I0-E2	20X (0.75)	48	48	10	4970.45
I0-E4	20X (0.75)	48	95	20	4970.45
I1-E1	20X (0.75)	119	24	2	12,426.12
I1-E8	20X (0.75)	119	14,316	20 * 30 frames	12,426.12
I2-E2	20X (0.75)	239	48	2	24,852.24
I2-E7	20X (0.75)	239	477	20	24,852.24
I3-E3	60X (1.2)	397	79	2	41,354.12
I4-E5	60X (1.2)	611	122	2	63,614.51

Table 1. Summary of laser exposure conditions tested in this study.

nonlinear optical imaging modalities, it is important to understand the effects of laser radiation on cell state, in order to properly interpret the transcriptomic measurement.

To address this need, this study aims to uncover the cellular response to pulsed laser excitation. Particularly, we investigate the effects of SRS, which is a multi-pulse technique that often reaches some of the highest photon fluxes commonly used. We investigated the effects of both single, and multiple excitation pulses, relevant to a broad range of nonlinear optical imaging modalities. We also performed measurements of reactive oxygen species and quantification of cell proliferation after exposure, for comparison with previous studies[11,13]. Critically, we tested for potential phototoxic effects in gene expression using RNA-seq, which allows for a transcriptome-wide assessment of potential changes caused by laser exposure. The results of this study provide comprehensive guidelines for minimizing the effects of phototoxicity in SRS imaging, and nonlinear imaging in general.

Results

Mechanism of laser-induced damage.
Photodamage induced by multiphoton microscopy includes both linear and nonlinear processes[12,18,19]. It has been suggested that, with lower laser peak power in CARS imaging, photodamage is dominated by linear dependence on peak power[12]. Whereas second order processes dominate at higher peak power[12]. The linear dependence of photodamage on peak power has been associated with one-photon absorption in human skin and *Escherichia coli*[12,20,21]. Linear and higher order processes can both lead to heating, but result in different profiles of temperature distribution where nonlinear absorption is mediated by free electrons[22]. Plasma generation through ionization, a result of the multiphoton process, can also have chemical effects in addition to thermal. The chemical effects include increase of ROS generation and fragmentation of biomolecules, e.g. DNA fragmentation and loss of membrane integrity[9,13,14,22]. ROS-mediated phototoxic effects were associated with thermal inactivation of ROS scavengers in cells, in addition to the increase in ROS generation[9]. In the same study, PCR arrays, immunoblotting, and ATF-knockdown were used to assess the role of ER stress pathway after laser irradiation[9]. Using a continuous-wave laser to achieve a fluency comparable to our study (around 27 J/cm²), Khan et al. only observed phototoxic effects in black wells that absorbed 100% laser irradiation but not in clear wells[9]. Our study used clear glass-bottom well plates to minimize the amount of laser irradiation absorbed by the well plates. Damage in DNA and the plasma membrane has been reported to result in apoptosis[13]. However, some studies found increase in ROS generation or apoptosis in cells exposed to laser without direct DNA damage[9,14]. Other observed cellular damages that did not directly lead to apoptosis include non-lethal morphological changes, loss of cloning efficiency and uncontrolled cell growth[11,15,18]. A summary of imaging conditions reported in the literature and the corresponding photodamage is listed in the Supplementary Table 1. Understanding the thresholds for these phototoxic effects is critical for designing a stimulated Raman scattering imaging experiment. We aimed to measure the transcriptome-wide response in N2A cells by performing bulk RNA-sequencing after exposure to femtosecond pulsed laser irradiation with different exposure settings. We also investigated both the immediate and long-time scale response by quantifying intracellular generation of ROS immediately after irradiation and by characterizing cell proliferation for 24 h after exposure.

Laser induced phototoxicity with typical SRS imaging conditions.
In stimulated Raman scattering (SRS) microscopy, as well as two-photon excitation microscopy (TPEF), many critical imaging parameters can influence the degree of photodamage on cells, including laser peak intensity, average intensity, repetition rate, excitation wavelength, total energy deposition on the samples, and Raman resonance[11,12,23]. We tested how the choice of parameters contributes to photodamage on Neuro2A (N2A) cells, a mouse neuroblastoma cell line. The imaging settings were chosen to represent typical settings of SRS imaging and were also comparable to settings used for TPEF (Table 1).

First, we tested the long-term effect of the average excitation intensity on N2A cells in two imaging experiments with identical cells, by tuning laser excitation power. The repetition rate and pulse width were kept constant at 80 MHz and 120 fs. Thus, the test was equivalent to comparing different laser peak intensities. N2A cells were exposed to a single 120-fs laser with an average power at the sample plane of 20mW and 100mW, corresponding to average intensities of 47.72 mW/μm² (exposure condition I0-E0; Table 1) and 238.58 mW/μm² (exposure condition I2-E2), respectively at 796 nm. After exposure, the proliferation rates of the N2A cells in each well were measured. Additionally, proliferation of negative control (NC) samples was measured simultaneously in
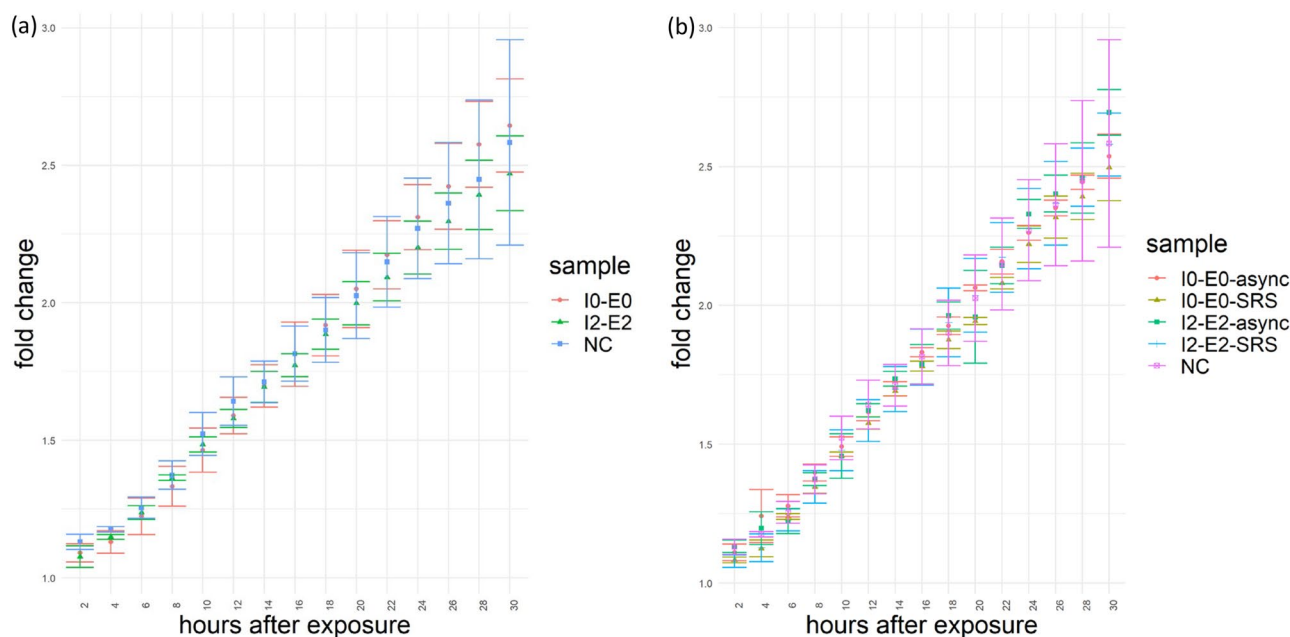
Figure 1. Proliferation rates after laser exposure measured as fold changes of the counts of N2A cells every 2 h with respect to the initial counts of cells immediately after the completion of all laser exposures. I0: average intensity = 47.72 mW/μm^2; I2: average intensity = 238.58 mW/ μm^2. E0: fluency = 9.54 J/cm^2; E2: fluency = 47.72 J/cm^2; NC = negative control; SRS: imaged with SRS; async: imaged with an interpulse delay of 50 ps. (**a**) A single pulsed laser at 796 nm was used. (**b**) Two lasers at 796 nm and 1040 nm were used, which had 1:1 power ratio, with the same total average intensities as the respective single laser settings.

adjacent wells that did not receive laser irradiation but were subjected to the same handling otherwise. For all samples, total cell counts were recorded every 2 h for 30 h starting about 10–20 min after exposure. Proliferation was calculated as the fold change in total cell count with respect to the initial counts of cells at the beginning of the proliferation assay. The proliferation rates of the two exposure conditions, I0-E0 and I2-E2, were identical to the negative control group during the 30 h after laser exposure (Fig. 1a), indicating that these intensity levels did not have adverse effect on the cloning efficiency of N2A cells.

In addition to the photo-damage caused by the combined power from two excitation sources, the coherent Raman scattering process can also induce photodamage by Raman resonance[12]. We tested if excitation with pump and Stokes wavelengths chosen to excite Raman resonance in CH$_3$ bonds would result in damage that perturbed proliferation rates. To do this, we added a second excitation source, while keeping the total combined intensity of the two sources equivalent to the previous settings. For each of the two intensities, 47.72 mW/μm^2 and 238.58 mW/μm^2, N2A cells were imaged with SRS by dividing the total intensities between two lasers at 796 nm and 1040 nm with 1:1 ratio (exposure condition I0-E0-SRS for 47.72 mW/μm^2 and I2-E2-SRS for 238.58 mW/μm^2). Representative SRS images of N2A cells were presented in Fig. S2. Although the combined intensities of the two lasers were the same as the intensities of single lasers in the previous tests (I0-E0 and I2-E2), half of the intensities were allocated to a longer wavelength at 1040 nm, which might affect the response of cells, in addition to the effects of Raman resonance. We exposed separate samples of N2A cells to the same two-laser settings but eliminated the Raman resonance by delaying the arrival time of the 1040 nm pulse by 50 ps with respect to the 796 nm pulse (exposure condition I0-E0-async for 47.72 mW/μm^2 and I2-E2-async for 238.58 mW/μm^2). We observed that neither condition diminished cell proliferation over the 30-h period immediately after laser exposure, comparing to the negative control cells that were not exposed to laser irradiation (Fig. 1b).

Although laser exposure did not negatively impact the long-term survival of N2A cells, this does not preclude the possibility of shorter timescale photo-induced perturbations that do not result in the change of proliferation rate. Such shorter timescale perturbations might be recorded in transcriptional activity which can capture many aspects of cellular changes and can change within minutes after perturbation[24]. To test for the potential changes in gene expression, we performed bulk RNA-seq on N2A cells that were exposed to the single-laser excitation settings tested in the proliferation assays (exposure condition I0-E0 and I2-E2). For each sample exposed to laser irradiation, RNA was extracted 1 h after exposure. The length of post-exposure incubation was chosen to allow sufficient time for transcriptional changes to occur before significant mRNA degradation, according to studies of mammalian cell transcription rate[24] and mRNA half-life[25]. We compared gene expression in the exposed cells to negative control samples that were not exposed to laser irradiation but were otherwise subjected to the same handling. We did not find any differentially expressed genes with a false discovery rate (FDR) < 0.05, after adjusting for multiple hypothesis testing with the Benjamini-Hochberg procedure[26] or with the Bonferroni correction[27] (Fig. 2a,b), indicating that these excitation intensities produced no significant perturbation to gene expression in N2A cells.
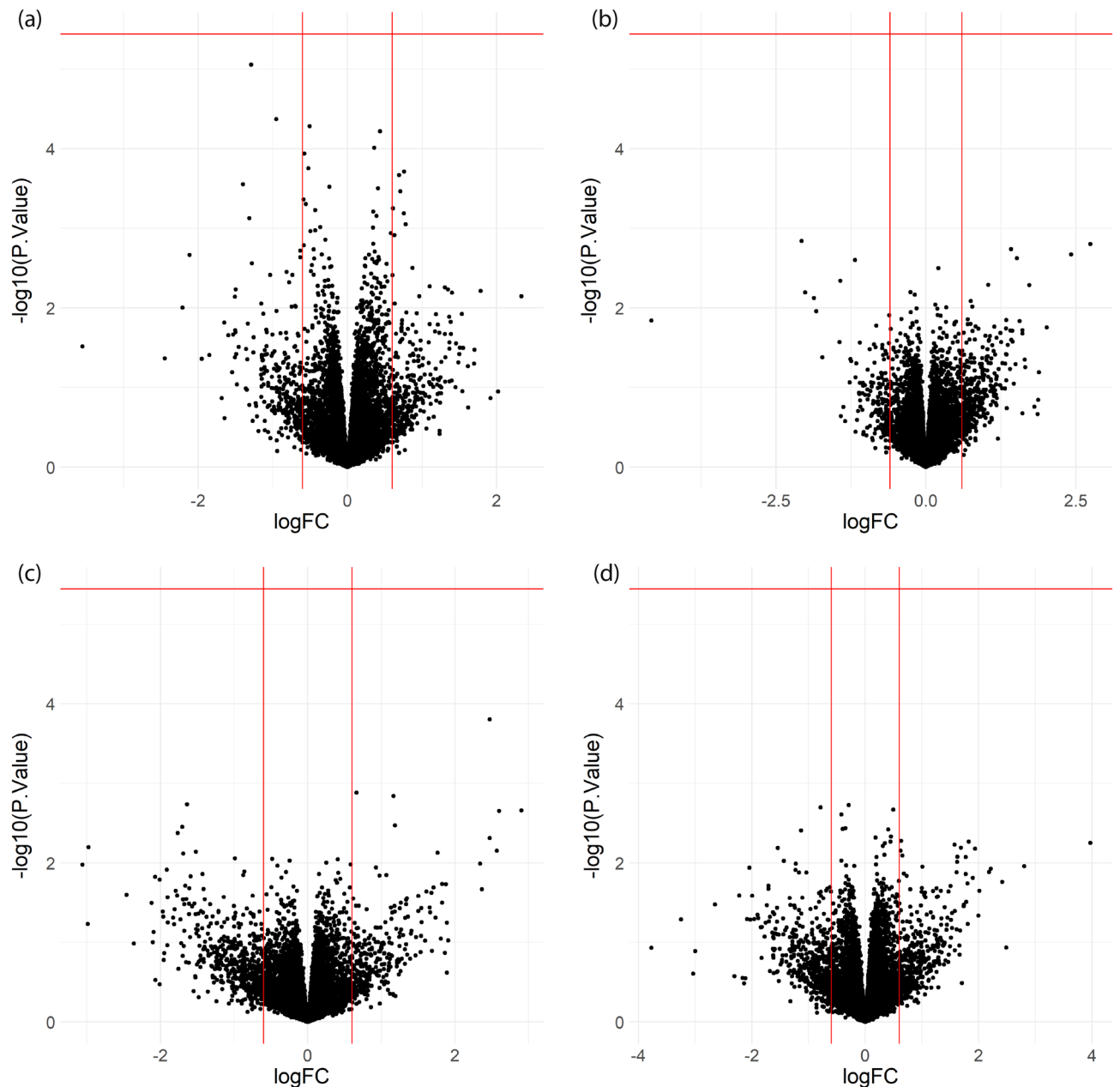
Figure 2. RNA-seq volcano plots of differential gene expression from single laser exposure conditions compared to the negative control samples. (**a**) I0-E0: average intensity = 47.72 mW/μm^2; fluency = 9.54 J/cm^2. (**b**) I2-E2: average intensity = 238.58 mW/μm^2, fluency = 47.72 J/cm^2. (**c**) I0-E2: average intensity = 47.72 mW/μm^2; fluency = 47.72 J/cm^2. (**d**) I0-E4: average intensity = 47.72 mW/μm^2, fluency = 95.43 J/cm^2. logFC: log2 fold change with respect to negative control samples (NC) that were not exposed to laser. Vertical lines are at −0.6 and 0.6. −log10(p-value): −log10 of p-values of differential expression with respect to NC. Horizontal lines indicate familywise error rate of 0.05 after Bonferroni correction[27].

In addition to laser excitation intensity and Raman resonance, the total energy deposition on the cells could also influence the extent of phototoxicity. This incident photon dose is determined by the excitation intensity and the total exposure time. In the context of laser scanning microscopy, slower scanning speeds or repeated imaging can increase photo-induced damage[12,23].

We tested the impact of increasing energy deposition per unit area (fluency) by increasing pixel-dwelling time given a fixed intensity. To achieve an increase in fluency of 5x and 10x, the pixel dwelling times were increased from 2 μs/pixel in the 47.72 mW/μm^2 samples (I0-E0) to 10 μs/pixel and 20 μs/pixel respectively (exposure condition I0-E2 and I0-E4; Table 1). We performed RNA-seq with the same procedure as in the previous test. Comparing to the negative control groups that did not undergo laser exposure, no significant differential gene expression was found in these two exposure groups either (Fig. 2c,d).

Laser-induced photo-toxicity with high-intensity SRS imaging. We did not observe any phototoxic effects on proliferation or gene expression with the typical SRS imaging parameters. However, in signal-limited SRS imaging applications much higher excitation intensities are often implemented, such as in the identification of the signature of neuronal membrane potentials[28]. In these scenarios, researchers must balance the large excitation intensities required for high-sensitivity SRS with photo-damage in the sample resulting from strong photo-absorption including plasma generation[12] and extreme heating[29]. This damage can often be observed visually as burning or boiling of the sample[30]. Thus, we probed the impact of laser absorption at settings that are close to causing sample destruction by heating. We increased the total average intensity to 397 mW/μm^2 by switching from a 20X to 60X objective with 1.2 NA. We chose a near-burning condition by repeatedly imaging the same field of view until burning was observed in some cells (Fig. S1), which occurred after 14 successive image scans, the equivalent of 1111.6 J/cm^2. In this setup, two lasers at 796 nm and 1040 nm with a 10:3 power ratio and 2 μs pixel dwelling time were used. In the subsequent experiments, we used the same setup but only scanned each field of view once (exposure condition I3-E3-SRS, Table 1). To test for the long-term survival, we performed a proliferation assay following the same procedure as in the previous section. No change was observed in the proliferation rate of N2A cells after exposure to this near burning condition using two lasers with 50-ps inter-pulse delay compared to the negative control group without laser exposure (Fig. 3b). Under identical laser settings, imaging using SRS with Raman resonance at 2950 cm^{-1} also did not change the proliferation rate of N2A cells (Fig. 3a). We tested for shorter time-scale perturbations by performing RNA-seq 1 h after imaging the N2A cells with SRS under the near-burning condition (I3-E3-SRS). No differentially expressed gene with a FDR < 0.05 were found in this condition comparing to the negative control group (Fig. 3c). This result suggests that N2A cells are robust to high-intensity laser exposure and vibrational excitation.

We increased the intensity further to probe the limits of non-perturbative femtosecond laser scanning excitation. With an average intensity of 610.7 mW/μm^2 at 796 nm (exposure condition I4-E5) and 2 μs pixel dwelling time, we observed cell burning starting around the second or third sequential imaging frame (equivalent to 244 to 366 J/cm^2). Under the same laser excitation condition but only one imaging frame, the samples exposed to laser irradiation had a proliferation rate that was significantly reduced (~ 25%) compared to the negative control samples without laser exposure (Figs. 3d, S3a). Laser-induced changes in N2A started to result in proliferation rate changes between average intensity of 397 mW/μm^2 with a fluency of 79.4 J/cm^2 and 610.7 mW/μm^2 with a fluency of 122 J/cm^2.

Photo-induced generation of reactive oxygen species in N2A cells. Generation of various reactive oxygen species (ROS) has been observed under a wide range of laser exposure conditions. The generation of ROS has been associated with sample ionization[12], heat generation[9], and active repair mechanism of cells[14]. Measurement of the generation of ROS is an additional approach for the investigation of photo-induced physiological perturbations in live cells, that occur on shorter timescales and that may not have observable influence on gene expression or proliferation rate. Although the causality between ROS generation and change in gene expression is unclear, such measurements can be used as an orthogonal measurement of photo-induced perturbations in live cells. We explored a series of increasing excitation intensities and pixel dwelling times that were used in the RNA-seq and proliferation assays as listed in Table 1. The increase in ROS generation was measured by the increase in the fluorescence of the CellROX Green dye, which became fluorescent after oxidation by ROS (Fig. 4a)[31]. Comparing to the negative control samples without laser exposure (Fig. 4g,h), the only condition that resulted in a significant ROS increase was I4-E5 (average intensity = 610.7 mW/μm^2, fluency = 122 J/cm^2; Fig. 4c,d), the near-burning condition we described in the previous section that also resulted in decreased proliferation rates. This is also the exposure condition with the highest intensity among all experiments. Other exposure settings tested did not result in significant generation of ROS measured by the CellROX Green dye. This includes the same exposure settings that did not result in changes of proliferation rates or differential gene expression measured by RNA-seq in the previous tests (exposure condition I0-E4, I2-E2, I3-E3; Figs. 4b–f, S3b,c). This observation confirms that these imaging conditions caused insignificant perturbations on the N2A cells. Additionally, we tested two conditions that had lower intensity but higher fluency than I4-E5, the condition with increased generation of ROS. First, we used the same intensity as I2-E2, 238.58 mW/μm^2, using 796 nm wavelength and 20X objective. The fluency was increased to 477.2 J/cm^2 by increasing the pixel dwelling time to 20 μs. This condition with 3.9 times higher fluency than I4-E5 did not result in significant ROS generation. We further increased the fluency to 14,316 J/cm^2 using an average intensity of 119.29 mW/μm^2 at 796 nm. The fluency was achieved by using a 20 μs pixel dwelling time and repeatedly imaging the same field of view 30 times. This 117 times increase in fluency from I4-E5 also did not cause in increase of ROS generation. Thus, intensity rather than fluency was observed to be the major factor that induced ROS generation in N2A cells after exposure to a pulsed laser excitation. If high imaging intensity is necessary, the addition of ROS scavengers, such as N-Acetyl-L-cysteine and Catalase, might protect cells from oxidative damage[9]. Lowering cell culture temperature during imaging has also been reported to reduce photodamage caused by exposure to continuous-wave lasers[9]. Additional experiments are needed to examine if the addition of oxygen scavengers or lowering temperature would result in changes of gene expression or other perturbations.

Discussion

This study assessed the effects of laser exposure on mouse Neuro2A cells during SRS imaging or other femtosecond pulsed laser-based imaging modalities that use similar excitation parameters. Multiple types of measurements were used—RNA-seq, proliferation assay, and ROS assay—to probe N2A cells at a range of time points after laser exposure. We demonstrated that N2A cells can have strong tolerance to laser exposure over a wide range of imaging power and intensity. This tolerance of N2A cells makes it possible to perform time-lapse
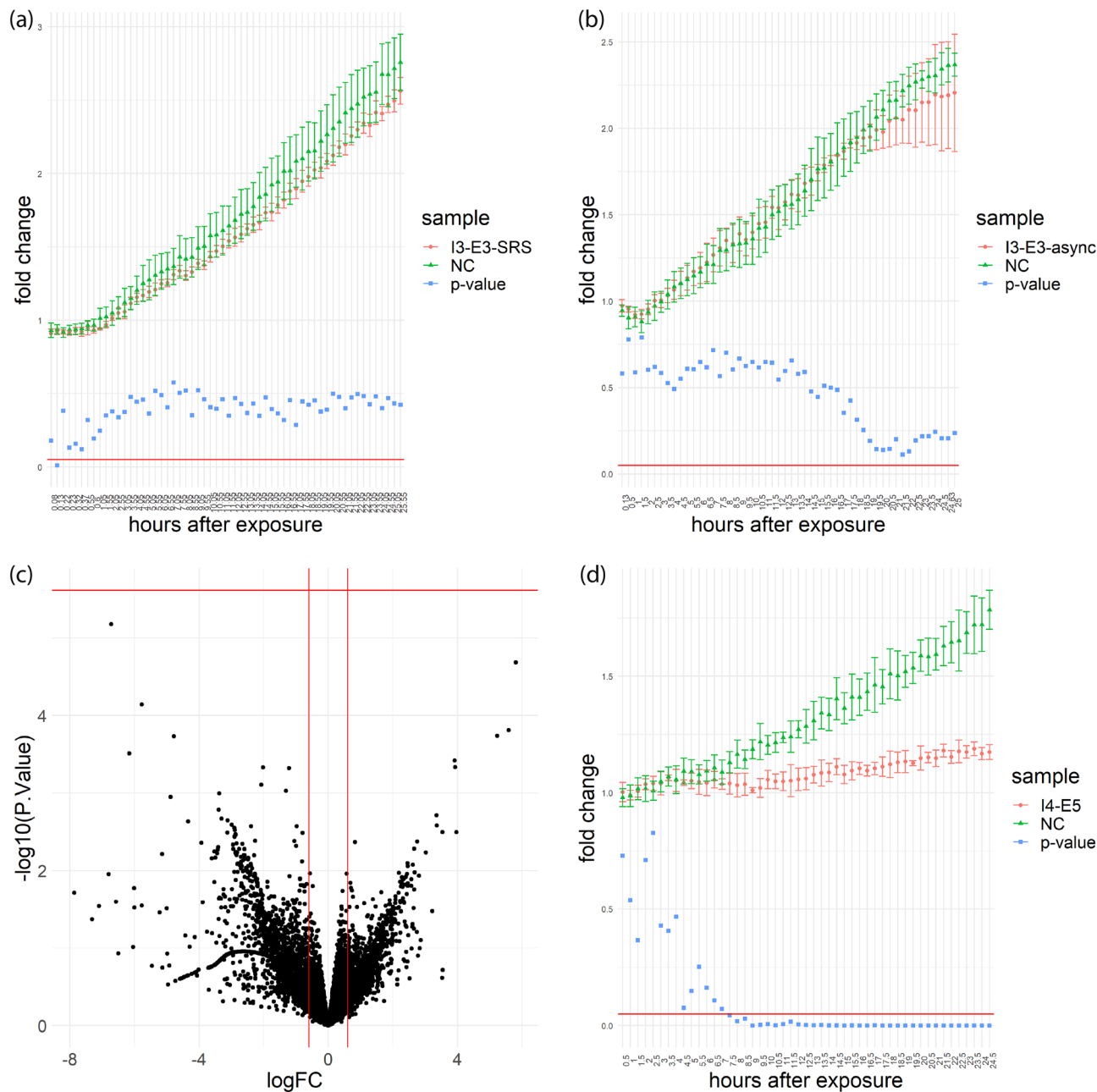
Figure 3. Proliferation and RNA-seq of near-burning conditions. (**a**) Proliferation rates of I3-E3-SRS measured as fold changes of the counts of N2A cells at every 30 min with respect to the initial counts of cells immediately after the completion of all laser exposures; (**b**) proliferation rates of I3-E3-async with the same laser settings as in (a) except a 50-ps interpulse delay; (**c**) RNA-seq volcano plot of I3-E3-SRS with respect to NC; (**d**) proliferation rates of I4-E5. I3: average intensity = 397 mW/μm^2; I4: average intensity = 610.7 mW/μm^2; E3: fluency = 79.4 J/cm^2; E5: fluency = 122 J/cm^2; NC = negative control. SRS: cells were imaged with SRS; async: cells were imaged with an interpulse delay of 50 ps. logFC: log2 fold change with respect to NC. Vertical lines are at −0.6 and 0.6. −log10(p-value): −log10 of p-values of differential expression with respect to NC. Horizontal lines indicate familywise error rate of 0.05 after Bonferroni correction[27].

imaging, RNA-seq, and other measurements after the first exposure to laser excitation without inducing biological perturbations in the downstream measurements. This allows for accurate interpretation of paired imaging and RNA-seq measurements, which could gain additional insights compared to the individual measurements alone. However, any RNA-seq measurements could only capture the state of gene expression at the time of the measurement. Although we chose the 1-h incubation time before RNA-seq to allow for sufficient time for potential transcriptomic changes to occur, gene expression changes might happen at a longer time scale, that was not captured in this study. The lack of change in the 1-h period after laser irradiation could potentially be indicative of the absence of other forms of cellular changes. However, it's possible that the response of N2A to laser exposure was reflected in changes unrelated to gene expression differences. This study focused on one particular cell type,
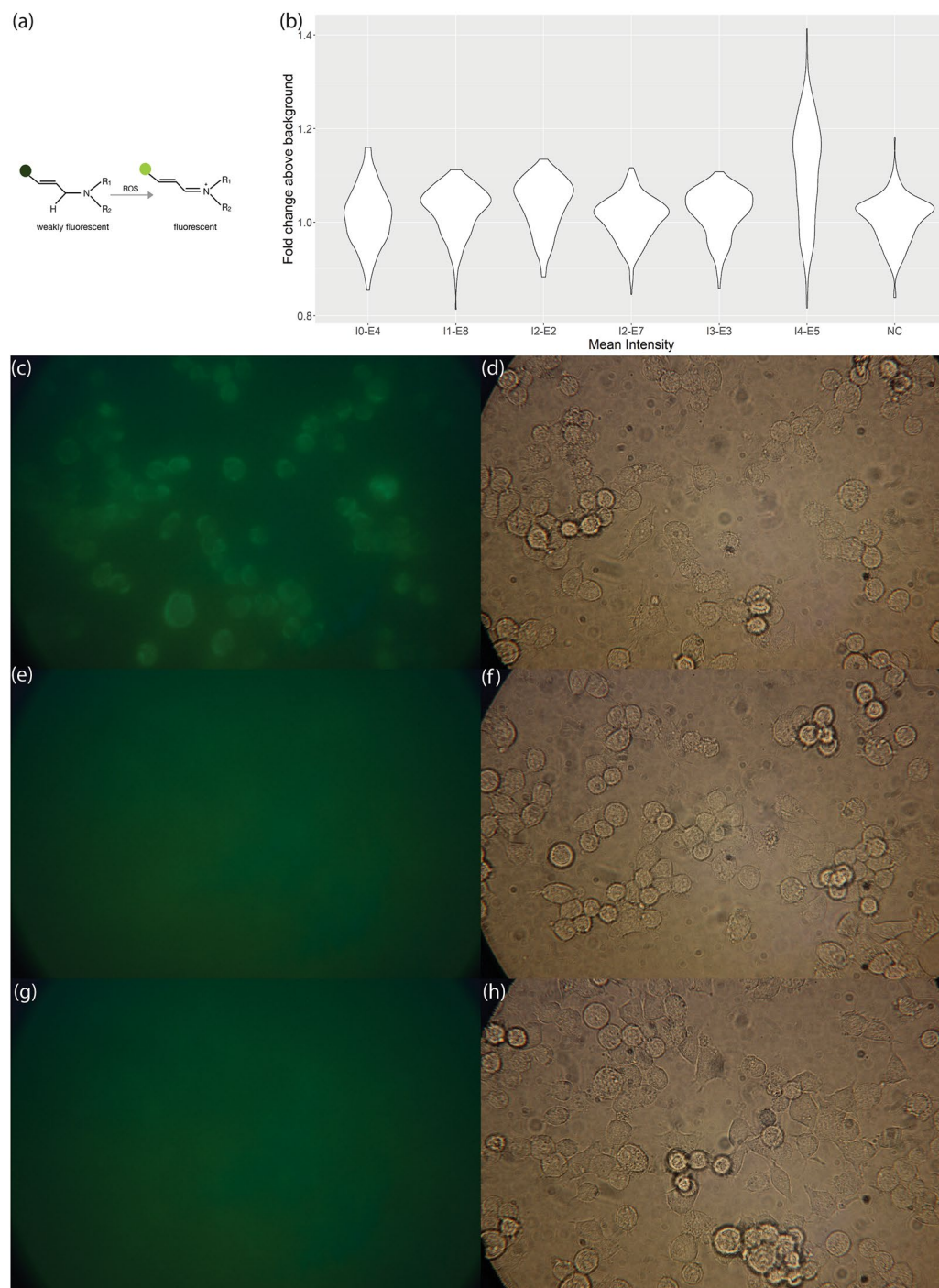
Figure 4. ROS measurements across laser intensities and fluencies. (**a**) Skeletal formula schematic of oxidation of CellROX Green dye by ROS[31]. (**b**) Distribution of mean intensities of all cells in samples with laser exposure and the negative control group after flatfield correction. *p*-value of I0-E4 versus NC is 0.0871. *p*-value of I1-E8 versus NC is 1.47e−5. *p*-value of I2-E2 versus NC is 2.89e−10. *p*-value of I2-E7 versus NC is 0.33. *p*-value of I3-E3 versus NC is 9.11e−4. *p*-value of I4-E5 versus NC is 5.73e−45. (**c**) GFP channel after exposure to I4-E5 and 30 min post-exposure incubation (**d**) Bright-field image of the same field of view as (c). (**e**) GFP channel after exposure to I3-E3 and 30 min post-exposure incubation (**f**) Bright-field image of the same field of view as (e). (**g**) GFP channel after 30 min incubation of unexposed cells (**h**) Bright-field image of the same field of view as (g). I0: average intensity = 47.72 mW/μm^2; I1: average intensity = 119.29 mW/μm^2; I2: average intensity = 238.58 mW/μm^2; I3: average intensity = 397 mW/μm^2; I4: average intensity = 610.7 mW/μm^2; E2: fluency = 47.72 J/cm^2; E3: fluency = 79.4 J/cm^2; E4: fluency = 95.43 J/cm^2; E5: fluency = 122 J/cm^2; E7: fluency = 477.2 J/cm^2; E8: fluency = 14,316 J/cm^2; NC = negative control.

N2A, and the response might differ from other cell types in their sensitivity and tolerance to laser exposure. The ROS assays also demonstrated that cells can have different tolerance to increase in laser excitation intensity and fluency, which could be a factor to consider when higher resolution is required (Fig. S3b,c). Except for I1-E8, where we repeatedly imaged N2A cells in the same field of view 30 times before the ROS assay, we did not explore the possibility of photo-induced perturbations caused by repeated exposure in other contexts. Changes in N2A cells might be observed with extended exposure beyond 20 μs/pixel and 1 imaging frame prior to RNA-seq or proliferation assay. The tunable parameters in SRS imaging form a multidimensional space that allow the imaging settings to vary widely among different applications. The subset of parameters we chose to assess aimed to cover representative changes in intensity, pixel dwelling time, wavelength, and vibrational resonance. Since we only observed increases in ROS generation and decreases in proliferation rate at the highest intensity condition with exposure to a single laser (I4-E5), thermal effects are likely the dominant damage mechanism for N2A cells when exposed to pulsed-laser excitation. Thermal effects without Raman resonance are known to have a first-order dependence on peak power[12,22]. Other studies of photodamage in the context of CARS and TPEF observed perturbations to cells using pico-second lasers and/or higher pixel dwelling time (e.g. 60 μs/pixel comparing to 2–20 μs/pixel in our study)[11–13]. Compared to imaging conditions previously reported to induce photodamage, imaging conditions in this study have comparable or higher average intensities but much lower fluency (Supplementary Table 1). Condition I1-E8 was used to test the impact of low intensity and higher fluency, and did not result in significant ROS generation. However, I1-E8 has lower average intensity than some of the intensity thresholds in the literature. This indicates that both intensity and fluency can lead to photodamage, and that either can be increased significantly without inducing damage, if the other is kept at lower values. Additionally, depending on the timing of downstream measurements, the impacts of laser excitation could manifest in different aspects of cellular processes. Photodamage observed using a particular measurement modality might not be observable with other modalities. Our multimodal measurements at representative timescales after laser exposure could provide insights for assessing potential impacts of laser exposure in future SRS imaging experiments.

Methods

Cell culture.
Neuro2A cells (N2A; UCB Cell Culture Facility) were cultured in T25 flasks using standard cell culture conditions for all experiments—37 °C, 5% CO_2, and complete growth medium consisting of DMEM (Gibco™ 10,566,016), 10% FBS (Avantor Seradigm 89,510), and 1% penicillin-streptomycin (Gibco™ 15,140,122). Cells were grown to approximately 80–90% confluency and one day prior to each imaging experiment, they were resuspended and seeded into 8-well glass-bottom μ-Slide (ibidi 80,827) for the ROS assays and into 384 glass-bottom well plates (Corning 4581) for the proliferation assays and RNA-seq. The growth medium for the ROS assays did not contain phenol red. At the start of each experiment, the confluency was approximately 40% for the proliferation assays and 70% for the ROS assays and RNA-seq.

Live-cell imaging and pulsed laser exposure.
The optical setup has been described previously[32]. The fundamental and tunable output from a commercially available femtosecond oscillator/OPO (Insight DS+, Spectra-Physics) was used as the excitation source. The OPO output was tuned to 796 nm for all measurements. The fundamental was at 1040 nm. For single-pulse measurements, only the OPO output at 796 nm was used. For two-pulse measurements the output from both the fundamental and OPO were used. Each line's power was controlled through the use of a variable attenuator consisting of a half-wave plate or half-wave fresnel rhomb (OPO output), and a polarizer, and set to the power specified in the main text. The inter-pulse delay was controlled by a delay stage (FCL200, Newport) on the tunable output line, and the two lines were combined on a 1000 nm short-pass dichroic mirror (Thorlabs), and fed into an inverted scanning microscope. (Olympus IX83-FV1200) A 20× objective with a numerical aperture of 0.75 (Olympus, UPLSAPO20X) or a 60× objective with a numerical aperture of 1.2 was used for all measurements, and frames were acquired at 512 × 512 pixels with a dwell time of 2 μs per pixel. The wavelength of 796 nm was chosen because when coincident with the fundamental 1040 nm line it provides the pump for a stimulated Raman interaction at a frequency of 2950 cm^{-1}, corresponding to CH3 stretches, largely found in proteins throughout the cell. In addition to SRS imaging, to deconvolve the contribution of the stimulated Raman process from the other effects of the dual laser excitation, measurements were acquired at an inter-pulse delay of 50 ps, with the 796 nm pulse arriving first.

The imaging power was measured with an optical power meter placed directly above the objective at the sample plane. To account for the difference in the magnification of different imaging conditions, we reported the average intensity calculated as the imaging power normalized by the beam size at the sample point (Table 1, avg intensity). The beam size is estimated by the Rayleigh criterion as 0.61 * wavelength / numerical aperture. We also provided the peak intensity in Table 1, which is the average intensity divided by the ratio of the actual exposure time in one second given the repetition rate and the pulse width. For our setup, the peak intensity was the average intensity * 1 s / (80 MHz * 120 fs).

ROS assay.
The N2A cells were exposed to the different settings as described in Table 1, with three replicates per exposure condition. The three negative control wells were not exposed. ROS generation was detected by CellROX™ Green reagent (Invitrogen) following the manufacturer's protocol. The dye was diluted to 5 μM in pre-warmed complete growth medium immediately before addition to cell culture. The growth medium in wells for exposure and the negative control wells was replaced by the medium with the dye in each well after the laser exposure for that well was completed, followed by 30 min incubation. After incubation, each well was washed three times with warm medium. A fluorescent image was taken in the GFP channel after the wash. A bright-field image of the same field of view was taken for each fluorescent image, so that the fluorescent increases post-exposure were normalized by the number of cells in each field of view. The same protocol was followed in empty wells

to confirm that the laser beams did not react with CellROX Green dyes directly to cause any fluorescent changes. Cell boundaries were manually defined using the bright-field images to measure fluorescence post-exposure. The fluorescence was normalized to the background by manually selecting regions in the same well that did not have cells. A flat-field correction was also applied to each fluorscence image. The reference for the flat-field correction was taken in empty wells with the same concentration of CellROX Green in warm complete medium under the same settings for the GFP channel. During all procedures, N2A cells were kept at 37 °C with 5% CO_2.

Proliferation assay. For each condition listed in Table 1, the entire culture wells in a 384 glass-bottom well plate were exposed to laser excitation by dividing each well into multiple non-overlapping fields of view. The stage was moved during the imaging of a well to scan each field of view once with the laser, such that all the cells in the same well were subjected to the same laser exposure condition. On the same 384-well plates, three wells of negative control cells were not exposed to the laser but were otherwise subjected to the same conditions. To measure the proliferation overnight with time-lapse imaging, we used IncuCyte ZOOM ((Essen BioScience) with a 10X objective to automatically acquire phase-contrast images while keeping the 384-well plates at 37 °C and 5% CO_2. A phase-contrast image was taken every 30 min to 2 h inside the IncuCyte for each well. N2A cells in the images were segmented using an algorithm for segmenting cells in bright-field images from Buggenthin et al. [33]. Fiji was used for counting cells in the binary images after segmentation[34].

RNA-seq. As in the proliferation assays, for each RNA-seq condition, the entire cell culture well in 384 glass-bottom well plates was exposed to laser excitation, such that all the cells in the same well were subject to the same laser exposure. The cells were lysed 1 h after laser exposure to allow sufficient time for transcriptional changes[35]. Three wells of unexposed cells subjected to the same conditions were lysed at the same time. We followed the manufacturer's protocol for RNA extraction (Qiagen RNeasy Mini Kit) and library preparation (NEBNext Ultra II RNA library prep kits for Illumina). Differential gene expression was tested for each exposure settings against the negative controls that were subject to the same ambient conditions and the same library preparation protocols but with no laser excitation. A false discovery rate < 0.05 was used as the threshold for differential expression after adjusting for multiple hypothesis testing with the Benjamini-Hochberg procedure[26] or with the Bonferroni correction[27]. The R package limma was used to perform this differential expression analysis[36].

Data availability

The sequencing datasets are available under the accession number GSE197666 (https://www.ncbi.nlm.nih.gov/geo/query/acc.cgi?acc=GSE197666).

References

1. Hoover, E. E. & Squier, J. A. Advances in multiphoton microscopy technology. *Nat. Photon.* **7**, 93–101 (2013).
2. Min, W., Freudiger, C. W., Lu, S. & Xie, X. S. Coherent nonlinear optical imaging: Beyond fluorescence microscopy. *Annu. Rev. Phys. Chem.* **62**, 507–530 (2011).
3. Hill, A. H. & Fu, D. Cellular imaging using stimulated raman scattering microscopy. *Anal. Chem.* **91**, 9333–9342 (2019).
4. Cheng, J.-X. & Xie, X. S. *Coherent Raman Scattering Microscopy* (CRC Press, 2016).
5. Cao, C., Zhou, D., Chen, T., Streets, A. M. & Huang, Y. Label-free digital quantification of lipid droplets in single cells by stimulated Raman microscopy on a microfluidic platform. *Anal. Chem.* **88**, 4931–4939 (2016).
6. Shi, L. *et al.* Mid-infrared metabolic imaging with vibrational probes. *Nat. Methods* **17**, 844–851 (2020).
7. Ji, M. *et al.* Rapid, label-free detection of brain tumors with stimulated Raman scattering microscopy. *Sci. Transl. Med.* **5**, 201 (2013).
8. Magidson, V. & Khodjakov, A. Circumventing photodamage in live-cell microscopy. *Methods Cell Biol* https://doi.org/10.1016/B978-0-12-407761-4.00023-3 (2013).
9. Khan, I., Tang, E. & Arany, P. Molecular pathway of near-infrared laser phototoxicity involves ATF-4 orchestrated ER stress. *Sci. Rep.* **5**, 1–14 (2015).
10. König, K., Liang, H., Berns, M. W. & Tromberg, B. J. Cell damage in near-infrared multimode optical traps as a result of multiphoton absorption. *Opt. Lett. OL* **21**, 1090–1092 (1996).
11. König, K., Becker, T. W., Fischer, P., Riemann, I. & Halbhuber, K.-J. Pulse-length dependence of cellular response to intense near-infrared laser pulses in multiphoton microscopes. *Opt. Lett. OL* **24**, 113–115 (1999).
12. Fu, Y., Wang, H., Shi, R. & Cheng, J.-X. Characterization of photodamage in coherent anti-Stokes Raman scattering microscopy. *Opt. Express OE* **14**, 3942–3951 (2006).
13. Tirlapur, U. K., König, K., Peuckert, C., Krieg, R. & Halbhuber, K. J. Femtosecond near-infrared laser pulses elicit generation of reactive oxygen species in mammalian cells leading to apoptosis-like death. *Exp. Cell Res.* **263**, 88–97 (2001).
14. Dillenburg, C. S., Almeida, L. O., Martins, M. D., Squarize, C. H. & Castilho, R. M. Laser phototherapy triggers the production of reactive oxygen species in oral epithelial cells without inducing DNA damage. *JBO* **19**, 048002 (2014).
15. König, K., So, P. T. C., Mantulin, W. W. & Gratton, E. Cellular response to near-infrared femtosecond laser pulses in two-photon microscopes. *Opt. Lett. OL* **22**, 135–136 (1997).
16. Chen, T. N., Gupta, A. N., Zalavadia, M. D. & Streets, A. μCB-seq: Microfluidic cell barcoding and sequencing for high-resolution imaging and sequencing of single cells. *bioRxiv* https://doi.org/10.1101/2020.02.18.954974 (2020).
17. Yuan, J., Sheng, J. & Sims, P. A. SCOPE-Seq: A scalable technology for linking live cell imaging and single-cell RNA sequencing. *Genome Biol.* **19**, 227 (2018).
18. Nan, X., Potma, E. O. & Xie, X. S. Nonperturbative chemical imaging of organelle transport in living cells with coherent anti-stokes Raman scattering microscopy. *Biophys. J.* **91**, 728–735 (2006).
19. Hopt, A. & Neher, E. Highly nonlinear photodamage in two-photon fluorescence microscopy. *Biophys. J.* **80**, 2029–2036 (2001).
20. Neuman, K. C., Chadd, E. H., Liou, G. F., Bergman, K. & Block, S. M. Characterization of photodamage to Escherichia coli in optical traps. *Biophys. J.* **77**, 2856–2863 (1999).
21. Masters, B. R. *et al.* Mitigating thermal mechanical damage potential during two-photon dermal imaging. *JBO* **9**, 1265–1270 (2004).

22. Vogel, A., Noack, J., Hüttman, G. & Paltauf, G. Mechanisms of femtosecond laser nanosurgery of cells and tissues. *Appl. Phys. B* **81**, 1015–1047 (2005).
23. Galli, R. *et al.* Intrinsic indicator of photodamage during label-free multiphoton microscopy of cells and tissues. *PLoS One* **9**, e110295 (2014).
24. Hargrove, J. L., Hulsey, M. G. & Beale, E. G. The kinetics of mammalian gene expression. *BioEssays* **13**, 667–674 (1991).
25. Sharova, L. V. *et al.* Database for mRNA half-life of 19 977 genes obtained by DNA microarray analysis of pluripotent and differentiating mouse embryonic stem cells. *DNA Res* **16**, 45–58 (2009).
26. Benjamini, Y. & Hochberg, Y. Controlling the false discovery rate: A practical and powerful approach to multiple testing. *J. R. Stat. Soc. Ser. B (Methodol.)* **57**, 289–300 (1995).
27. Dunn, O. J. Multiple comparisons among means. *J. Am. Stat. Assoc.* **56**, 52–64 (1961).
28. Lee, H. J. *et al.* Label-free vibrational spectroscopic imaging of neuronal membrane potential. *J. Phys. Chem. Lett.* **8**, 1932–1936 (2017).
29. Schönle, A. & Hell, S. W. Heating by absorption in the focus of an objective lens. *Opt. Lett.* **23**, 325–327 (1998).
30. Zhu, Z. *et al.* Using AIE luminogen for long-term and low-background three-photon microscopic functional bioimaging. *Sci. Rep.* **5**, 15189 (2015).
31. Invitrogen. Shedding light on oxidative stress: CellROX™ deep red reagent for ROS detection - US. In *Bioprobes 68* 7 https://www.thermofisher.com/content/dam/LifeTech/migration/en/filelibrary/support/bioprobes/bioprobes-64.par.27568.file.dat/bioprobes-64-cellrox.pdf. (2011).
32. Kim, S., Dorlhiac, G., Chaves, R. C., Zalavadia, M. & Streets, A. Paper-thin multilayer microfluidic devices with integrated valves. *Lab Chip* **21**, 1287–1298 (2021).
33. Buggenthin, F. *et al.* An automatic method for robust and fast cell detection in bright field images from high-throughput microscopy. *BMC Bioinform.* **14**, 297 (2013).
34. Schindelin, J. *et al.* Fiji: An open-source platform for biological-image analysis. *Nat. Methods* **9**, 676–682 (2012).
35. Shamir, M., Bar-On, Y., Phillips, R. & Milo, R. SnapShot: Timescales in cell biology. *Cell* **164**, 1302-1302.e1 (2016).
36. Ritchie, M. E. *et al.* limma powers differential expression analyses for RNA-sequencing and microarray studies. *Nucleic Acids Res.* **43**, e47–e47 (2015).

Acknowledgements

Author contributions

A.S. and X.Z. designed the study. X.Z. and G.D. performed experiments. G.D. designed and assembled the SRS microscope. X.Z. analyzed data. M.L. and A.S. supervised the research.

Competing interests

The authors declare no competing interests.

Additional information

Supplementary Information The online version contains supplementary material available at https://doi.org/10.1038/s41598-022-23054-7.

Correspondence and requests for materials should be addressed to A.S.

Reprints and permissions information is available at www.nature.com/reprints.

Publisher's note Springer Nature remains neutral with regard to jurisdictional claims in published maps and institutional affiliations.